

Luminous Change of Rhodamine 3B Incorporated into Titanate Nanosheet/Decyltrimethylammonium Hybrids under Humid Atmosphere

Ryo Sasai,*[1,†] Nobuo Iyi,[2] and Hiroki Kusumoto[1]

[1]Department of Applied Chemistry, Graduate School of Engineering, Nagoya University, F3-3(250), Furo-cho, Chikusa-ku, Nagoya 464-8603

[2]National Institute for Materials and Science (NIMS), 1-1 Namiki, Tsukuba 305-0044

Received December 7, 2010; E-mail: rsasai@riko.shimane-u.ac.jp

In this paper, the structural and spectroscopic properties of rhodamine 3B (R3B) cations incorporated into titanate nanosheet (TNS)/decyltrimethylammonium (C10TMA) cation hybrid was investigated in the presence and absence of adsorbed water. Powder X-ray diffraction measurement under various relative humidity indicated that the TNS/C10TMA/R3B hybrid had at least two water-adsorption sites with different affinity for water in the 2D nanospace of TNS stacked structure. Intensity reduction and blue shift in diffuse reflectance and photoluminescence spectra of the TNS/C10TMA/R3B hybrid powder was observed by water adsorption. This spectroscopic behavior could be explained as lowering of electrostatic interaction between the cation group of R3B and cation exchange sites on the TNS surface.

Ion exchangeable layered inorganic compounds are promising materials for the stability and solidification of functional organic materials because various ionic and polar organic compounds can be easily incorporated into the 2-dimensional (2D) interlayer nanospace via an ion-exchange reaction and enlargement of the interlayer clearance. Moreover, incorporated molecules spontaneously form an ordered structure such as a self-assembled bilayer. Thus, solid materials with anisotropic, nonlinear, and nonequilibrium properties can be easily prepared. Considering these useful characteristics, many studies have been conducted to evaluate the hybridization of various functional organic compounds with ion exchangeable layered inorganic compounds.[1–54]

Recently, we reported that a way to prepare layered inorganic hosts/rhodamine dye cation nanohybrids with high emission quantum yield, ϕ (max value: about 80%, incorporated dye concentration $\geq 10^{-2}$ mol dm^{-3}) could be established.[23,26,43] In this hybrid system, cointercalated alkyltrimethylammonium cations play an important role by acting as inhibitors of intermolecular interaction among incorporated dye cations in the host interlayer nanospace. We already reported that this preparation method for photoluminous solid materials could be applied to various layered inorganic host systems such as smectite, layered double hydroxide, and layered metallic salts.[1–54]

Generally, such ion exchangeable layered materials can adsorb a large amount of water within the interlayer nanospace.[5] In particular, it is well known that cation exchangeable layered clays can be easily exfoliated to a sheet of clay nanosheet. Moreover, a small amount of adsorbed water exists in the interlayer nanospace, even when interlayer space is modified by amphiphilic compounds such as surfactant. The effect of adsorbed water on the structural, physical, and chemical properties of various clay materials has been extensively studied.[4,5] Recently, Sasaki et al. reported that layered sodium cobaltate ($Na_{0.75}CoO_2$) exhibited superconductivity at low temperature (several kelvin) by the existence of water molecules hydrated to incorporated sodium ions and/or oxonium ions.[55,56] These previous reports indicate the possibility that the adsorbed or hydrated water can largely affect not only various properties of layered inorganic host but also that of layered inorganic host/photofunctional organic cation nanohybrids.

In this paper, the structural and photoluminous properties of titanate nanosheet/decyltrimethylammonium/rhodamine 3B nanohybrid powder were investigated in the absence and presence of adsorbed water in the interlayer nanospace. From various measurements, the following facts could be found: (1) the present nanohybrid has at least two adsorption site of water, (2) both emission and diffused reflectance spectra of the present nanohybrid exhibit a blue shift in the presence of adsorbed water, and (3) water adsorption on the titanate nanosheet surface would cause weakening of the electrostatic interaction between the cation of rhodamine 3B and anion site on the titanate nanosheet.

Experimental

Preparation. A titanate nanosheet (TNS) colloid suspension was prepared using a method described by Sasaki et al.[57] The detailed procedures is as follows: (1) cesium layered titanate (Cs-LT), $Cs_{0.7}Ti_{1.825}\square_{0.1725}O_4$ (□: Ti defect), was prepared by mixing Cs_2CO_3 powder purchased from Rare

† Present address: Department of Materials Science, Interdisciplinary Faculty of Science and Engineering, Shimane University, 1060 Nishi-kawatsu-cho, Matsue 690-8504

Published on the web May 7, 2011; doi:10.1246/bcsj.20100343

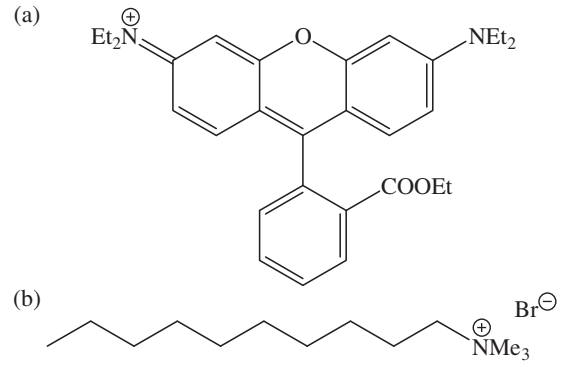

Scheme 1. Chemical structure of (a) R3B and (b) C10TMABr.

Metallic Co., Ltd. and TiO_2 (*anatase*) purchased from the Kojundo Chemical Laboratory Co., Ltd. (Cs:Ti = 2:5.3 molar ratio) via two calcinations at 1073 K for 20 h each. (2) Protonation of Cs-LT was then conducted by immersing 0.8 g of Cs-LT powder in 200 cm^3 of HCl aqueous solution (1.0 mol dm^{-3}) four times, which yielded protonated layered titanate (H-LT: titanic acid), $H_{0.7}Ti_{1.825}\square_{0.1725}O_4$. (3) A TNS colloid suspension was then prepared by magnetically stirring 150 cm^3 of tetrabutylammonium hydroxide (TABOH: purchased from Wako Pure Chemical Industries, Ltd.) aqueous solution (0.53 mol dm^{-3}) with wet H-LT for 5 days. The obtained TNS colloid suspension was a semitransparent white solution with a density of 3.3 g dm^{-3}.

Next, 0.5 dm^3 of a mixed aqueous solution of rhodamine 3B (R3B: purchased from Exiton. See Scheme 1a) and decyltrimethylammonium bromide (C10TMABr: purchased from Wako Pure Chemical Industries, Ltd. See Scheme 1b) was added to 1.1 g dm^{-3} of the TNS colloid suspension and then magnetically stirred at rt for 1 h. The amount of R3B and C10TMABr added was 0.02% and 100%, respectively, against the cation exchangeable capacity (CEC) of H-LT (4.12 mequiv g^{-1}). After filtration under reduced pressure and rinsing with distilled and deionized water, the TNS/C10TMA/R3B hybrid powders were obtained by drying at 333 K under reduced pressure overnight. For characterization, all hybrid powders were dried at 303 K for 2 h under vacuum prior to each measurement.

Characterization of TNS/C10TMA/R3B Powder. The amount of R3B incorporated into TNS/C10TMA/R3B was calculated from the absorbance at the peak wavelength ($\lambda = 560$ nm) of R3B in the filtrate recorded with a UV–vis spectrophotometer (V-550, JASCO).

The amount of incorporated C10TMA and residual TBA cations were evaluated by solving the following simultaneous equations based on the chemical amount of carbon (m^C) and nitrogen (m^N) in the sample powder estimated from carbon–nitrogen–hydrogen (CHN) elemental analysis (MTA-620, Yanaco). Here, a contribution of incorporated R3B cation was already removed from both m^C and m^N.

$$x + y = m^N \quad (1)$$

$$(n + 3)x + 16y = m^C \quad (2)$$

where x and y are the chemical amount of C10TMA and TBA cations in the sample powder, respectively. As a result, the residual TBA cation was less than 1% vs. CEC, therefore the effect of residual TBA cations on the structural and functional features of the TNS/C10TMA/R3B hybrids could be neglected.

To estimate the basal spacing, d, of the sample powders, X-ray diffraction (XRD) analysis of the sample powders was carried out on a powder diffractometer (RINT 2500, RIGAKU) with Ni-filtered Cu Kα radiation (50 kV and 100 mA) under ambient conditions.

It is very difficult to measure the diffuse reflectance (DR) spectrum of powders with higher luminous intensities using a conventional UV–vis spectrometer, even when there is an integrating sphere system. This is because spectroscopy systems for reflected light from powder are not generally available in conventional UV–vis spectrometer, therefore the detected reflected light includes the emission light. As a result, the value of the Kubelka–Munk (KM) function will be underestimated. To accurately evaluate the DR spectrum, the synchronization mode of a fluorospectrometer (FP-6600, JASCO) attached to an integrating sphere unit was used. In this method, the DR spectrum of each sample powder was measured using the following procedures: (1) the synchronization spectrum of the reference sample (white slide) was measured. (2) The synchronization spectrum of the luminous powder sample was measured. (3) The difference in the spectra of (1) and (2) was converted into the KM function, and the value obtained corresponded to the absorption spectrum of the luminous sample powder.

The photoluminescence (PL) spectra of the sample powders were measured by using a fluorophotometer (FP-6600, JASCO) attached to a powder sample holder at an excitation wavelength, λ^{ex}, of 520 nm at rt under ambient conditions.

The PL quantum yield, ϕ, of hybrid powders was evaluated using an absolute PL quantum yield measurement apparatus (C9920-02, Hamamatsu Photonics) at $\lambda^{ex} = 540$ nm. It is usually difficult to measure the ϕ of luminous powder; however, this apparatus enables measurement of the photon number of both excitation light absorbed by the sample powder and the PL light from the luminous powder. Therefore, the absolute ϕ of the luminous powder can be estimated without using a standard sample.

Characterization under Humid Conditions. To investigate both structural and spectroscopic characteristics of the TNS/C10TMA/R3B powder adsorbed water molecules, various measurements of the TNS/C10TMA/R3B powder were conducted.

Adsorbed amount of water was estimated from weight change by measuring sample weight under given RH condition at 298 K.

To determine the dependence of the d value on the relative humidity (RH), XRD measurements were conducted using a powder diffractometer (RINT 1200, RIGAKU) equipped with an RH-controlled chamber under various RH conditions at 298 K. The measurements were conducted using Ni-filtered Cu Kα radiation. In addition, RH-controlled N_2 gas was supplied to the chamber from a RH-controlled gas supplier (SRG-1R-1, Shin-ei). The RH value was then monitored using

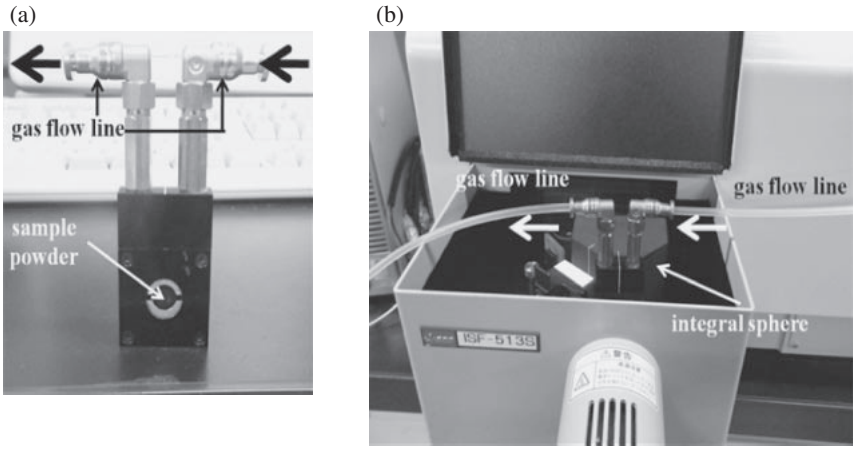

Figure 1. Photographs of (a) custom-made powder sample holder with gas flow line and (b) the instrumentation setting for measuring in situ DR and PL spectra of hybrid powders under dry and humid conditions.

a RH indicator (HMI41, Vaisala). After keeping the TNS/C10TMA/R3B powder under continuous N_2 flow for 1 h, the RH was increased stepwise up to 90% RH. The sample was maintained at each RH for 15–20 min, after which the XRD profile of the treated powder was recorded.

To investigate the spectroscopic features of TNS/C10TMA/R3B powder with water molecules, absolute ϕ was measured under the same conditions of the dried hybrid powders (cf. *characterization of TNS/C10TMA/R3B powder section*). To accomplish the water adsorption, TNS/C10TMA/R3B powder with water molecules was prepared by placing the dried TNS/C10TMA/R3B powder under humid conditions for 2 h at room temperature.

The PL and DR spectra of TNS/C10TMA/R3B powder with water molecules were measured with a fluorophotometer (FP-6600, JASCO) attached to an integrating sphere unit, and custom-made powder sample cell with gas-injection port (Figure 1a) was used as sample cell. The PL and DR spectra were measured by the following procedures: (1) after setting the cell with TNS/C10TMA/R3B powder on the apparatus like Figure 1b, dried N_2 gas was flowed for 60 min at 30 $cm^3\,min^{-1}$. (2) The PL and DR spectra of dried TNS/C10TMA/R3B powder were measured in the same way (cf. *characterization of TNS/C10TMA/R3B powder section*). (3) Humid N_2 gas, which was produced by putting through dried N_2 gas to pure water, were injected to the cell with TNS/C10TMA/R3B powder for 40 min at 30 $cm^3\,min^{-1}$. (4) The PL and DR spectra of TNS/C10TMA/R3B powder with sufficient water were measured. During this series of experimentals, the charged TNS/C10TMA/R3B powder was not changed, and thus, the DR spectra intensity of the TNS/C10TMA/R3B powder with water molecules can be compared to that of dried TNS/C10TMA/R3B powder.

Results and Discussion

Chemical Composition of TNS/C10TMA/R3B Hybrid Powder. From absorbance at 560 nm and CHN analysis, it was found that the prepared TNS/C10TMA/R3B hybrid powder has 0.02% R3B vs. CEC and 48% C10TMA vs. CEC. Moreover, CHN analysis showed almost no residual TBA cations in TNS/C10TMA/R3B hybrid powder. Therefore, the chemical formula of TNS/C10TMA/R3B hybrid dried powder was estimated to be $(C10TMA)_{0.28}(R3B)_{0.00014}H_{0.41986}Ti_{1.825}\square_{0.1725}O_4 \cdot H_2O$ (□: Ti vacancy). From this, the average intermolecular distance of R3B and C10TMA was calculated to be about 45 nm and about 1 nm, respectively. From these calculated values it could be easily expected that there are hardly any intermolecular interactions among R3B cations in the interlayer space in stacked TNS structure.

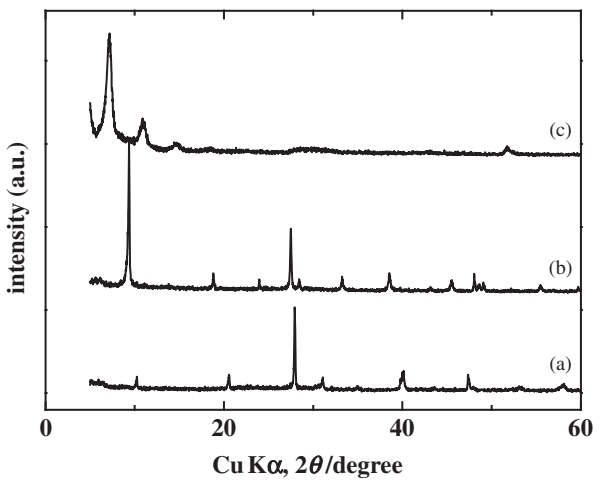

Figure 2. XRD patterns of the (a) Cs-LT, (b) H-LT, and (c) dried TNS/C10TMA/R3B hybrid powder.

XRD Analysis of TNS/C10TMA/R3B Hybrid Powder. Figure 2 shows the XRD patterns of the (a) Cs-LT, (b) H-LT, and (c) dried TNS/C10TMA/R3B hybrid powder. The XRD patterns of Cs-LT and H-Lt agreed well with the data available in the literature.[46] These results indicate that synthesis of the host inorganic compounds was achieved. The basal diffraction lines of the TNS/C10TMA/R3B powder could be observed at a lower angle than those of H-LT, indicating that a laminate structure of TNS such as Cs-LT or H-LT would be formed by intercalating both C10TMA and R3B as cation for charge compensation. From this basal diffraction line, the basal spacing, d, of TNS/C10TMA/R3B was 2.40 nm, and then, the interlayer clearance, D, was calculated as 1.80 nm, considering thickness of TNS layer (0.6 nm).[58] The alkyl chain of the

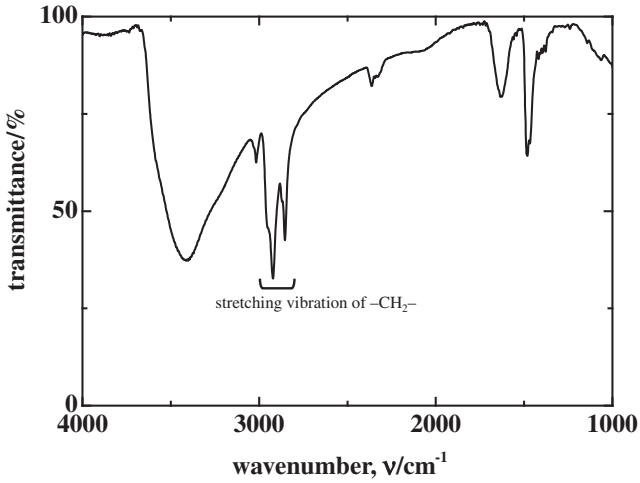

Figure 3. FT-IR spectrum of the dried TNS/C10TMA/R3B hybrid powder.

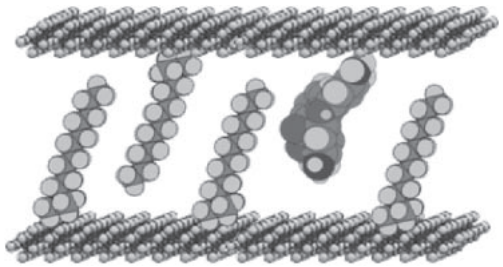

Figure 4. Schematically structural model of the dried TNS/C10TMA/R3B hybrid.

incorporated C10TMA cations has an all-*trans* configuration from both stretching vibrations of symmetry (2853 cm^{-1}) and asymmetry (2920 cm^{-1}) for methylene groups (Figure 3).[59] Thus, it is possible to estimate the molecular length of C10TMA to be 1.82 nm. From these values, it can be concluded that the C10TMA cations were aligned almost perpendicular to the TNS surface (Figure 4). The areas occupied by an anionic site on TNS surface and a C10TMA cation were $a(\mathrm{TNS}) = 0.32\,\mathrm{nm}^2$ and $a(\mathrm{C10TMA}) = 0.23\,\mathrm{nm}^2$, respectively. That occupied by a R3B cation was from a(R3B, perpendicular orientation to TNS surface) $= 0.58\,\mathrm{nm}^2$ to a(R3B, parallel orientation to TNS surface) $= 2.58\,\mathrm{nm}^2$ because R3B has various possibility for molecular orientation. Considering the incorporation amount of C10TMA and R3B cations, there was sufficient 2D interlayer nanospace in TNS/C10TMA/R3B hybrid regardless of the orientation of R3B ($a(\mathrm{TNS}) > (x/100) \times a(\mathrm{C10TMA}) + (y/100) \times a(\mathrm{R3B})$: x and y are incorporation rate of C10TMA and R3B).

The basal diffraction of TNS/C10TMA/R3B hybrid powder shifted toward a lower diffraction angle as the RH increased (Figure 5). These results indicate that the TNS/C10TMA/R3B hybrid swelled as a result of the adsorption of water molecules into the interlayer nanospace. Figure 6 shows the dependence of both d and adsorbed amount of water (n) on the RH. The d values exhibited a two-step dependence on RH as follows: (1) a rapid increase in d was observed up to 20%RH. (2) A plateau was observed from 20 to 40%RH. (3) The d value gradually increased as the RH increased at more than 40%RH. These

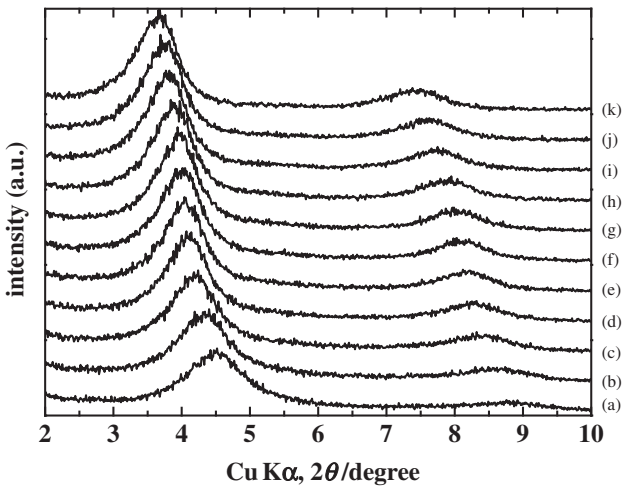

Figure 5. XRD patterns of the TNS/C10TMA/R3B hybrid powder under various RH: (a) dried (1%RH), (b) 3, (c) 10, (d) 20, (e) 30, (f) 40, (g) 50, (h) 60, (i) 70, (j) 80, and (k) 90%RH.

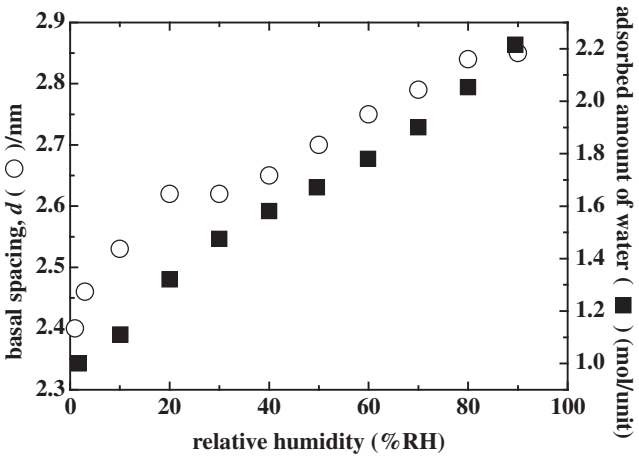

Figure 6. RH-dependence of basal spacing, d, (left axis) and adsorbed amount of water per chemical formulas (right axis) of TNS/C10TMA/R3B hybrid powder.

facts indicate that there are at least two water adsorption sites with different adsorption equilibrium constants. One adsorption site, which works at a lower RH (<20%RH), would have high affinity for water molecules, because the dependence of d on RH (Figure 6) exhibited a steep increase similar to a *Langmuir*-type adsorption isotherm. In the TNS/C10TMA/R3B hybrid powder, the near-field of the TNS layer surface can be considered a possible adsorption site. Usually, water molecules adsorbed on the oxide surface are strongly fixed by a hydrogen bond with the hydroxy group on the metal oxide surface. Thus, it can be concluded that expansion of the interlayer space observed at less than 20%RH is caused by water adsorption to the TNS layer surface, and this adsorption becomes saturated at about 20%RH. The gradual increase in d observed at more than 40%RH after water adsorption on TNS layer surface reached saturation could be caused by random water adsorption. It should be understood that the change in tilt angle of the alkyl chain of C10TMA and/or xanthene-ring of R3B cations by water adsorption was also one reason for such tendency, but the

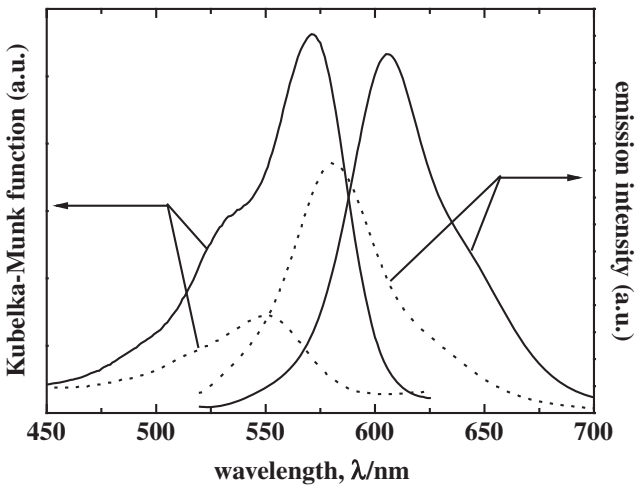

Figure 7. DR and PL spectra of TNS/C10TMA/R3B hybrid powder under dry (solid lines) and humid (broken lines) conditions.

contribution of this orientation change of incorporated cations will be small.

The *n* values also exhibited a two-step dependence on RH the same as the *d* values. This hybrid powder had 1 mol of water molecule per chemical formula of TNS/C10TMA/R3B under dried conditions. The *n* value became about 1.6 mol of water at 40%RH, and then became 2.2 mol of water molecule at about 90% RH. From these results, it was found that the capacity for water adsorption of the TNS/C10TMA/R3B hybrid was about 2.2 mol of water per chemical formula, of which 1.6 mol of water was adsorbed on the near-field of the TNS layer surface and residual water was randomly adsorbed in the interlayer space.

Spectroscopic Properties of TNS/C10TMA/R3B Hybrid Powder. Figure 7 shows the DR and PL spectra of TNS/C10TMA/R3B hybrid powder under dry and humid (RH is about 50%RH) atmosphere, respectively. From comparison of both DR and PL spectra shape between the dried TNS/C10TMA/R3B hybrid powder and monomeric R3B cations dissolved in an aqueous solution, it could be found that the R3B cations existed as monomer in the TNS/C10TMA/R3B hybrid. However, the peak wavelength (602 nm) was shifted toward the longer wavelength range than that of monomeric R3B dissolved in an aqueous solution (584 nm). Generally, such red shift will be interpreted as J-type aggregation formation of R3B cations. However, in the present case, it is hard to explain this red shift as J-type aggregation from the following two facts: (1) there is enough average intermolecular distance of the incorporated R3B cations (about 45 nm), and large part of interlayer space was occupied by the incorporated C10TMA cations. (2) The present TNS/C10TMA/R3B hybrid powder exhibited higher emission quantum yield, ϕ (68%. ϕ of R3B aqueous solution (1.0×10^{-6} mol dm^{-3}) exhibited as about 90%.). This is that the incorporated R3B cations exist as monomer in the dried TNS/C10TMA/R3B hybrid. Bujdák et al.[24] and Arbeloa et al.[60,61] previously reported that such red shift was observed in the dye–clay hybrid system, and such phenomena is caused by the strong electrostatic interaction between dye and clay anion-sites. Therefore, the red shift observed in the present TNS/C10TMA/R3B hybrid in dried state is also caused by the strong electrostatic interaction between monomeric R3B cation and a cation-exchange site on TNS surface.

In the DR and PL spectra of the water-adsorbed TNS/C10TMA/R3B hybrid powder, both blue shift and intensity reduction was observed. The shapes and mirror relationship between DR and PL spectra of the water-adsorbed TNS/C10TMA/R3B hybrid powder agree well with that of the monomeric R3B dissolved in an aqueous solution. Moreover, the ϕ value of the water-adsorbed TNS/C10TMA/R3B hybrid powder was 60%, and this ϕ value was approximately the same as that of the dried TNS/C10TMA/R3B hybrid powder. These findings indicate that incorporated R3B cations also exist as monomer in the water-adsorbed TNS/C10TMA/R3B hybrid. Thus, it is also found that the C10TMA cations effectively act as inhibitor of the intermolecular interaction among R3B cations incorporated in interlayer 2D nanospace of the TNS stacked structure, even when water molecules are adsorbed into TNS/C10TMA/R3B hybrid.

Here, the observed peak wavelength of DR and PL spectra of the water-adsorbed TNS/C10TMA/R3B hybrid powder ($\lambda^{abs} = 550$ nm and $\lambda^{PL} = 586$ nm) was almost the same as that of monomeric R3B cations dissolved in aqueous solution ($\lambda^{abs} = 560$ nm and $\lambda^{PL} = 584$ nm). This fact suggests that the strong electrostatic interaction between the cationic group of R3B cation and cation-exchange site on the surface of TNS layer is weakened or diminished by water adsorption, which occurs between the cationic group of R3B cation and cation-exchange site on the surface of TNS layer. The rapid increase in *d* value up to 20%RH observed in XRD profiles (Figure 6) supports this consideration.

Like the blue shift of the DR and PL spectra of the water-adsorbed TNS/C10TMA/R3B hybrid powder, the decrease in the intensity of DR and PL spectra was also observed by water adsorption. It can be predicted that this intensity reduction of DR and PL spectra observed in the water-adsorbed TNS/C10TMA/R3B hybrid powder can be explained as follows: (1) abundance of monomeric R3B cations with luminescence decreased for some reason, for example, a part of R3B cations were converted to lactone without luminescence by intramolecular cyclization. (2) The molecular orientation of the incorporated R3B cations in the TNS/C10TMA/R3B hybrid is changed from specific alignment to random fashion by water adsorption. This phenomenon will cause a decreased molecular absorption cross section, that is, the apparent molecular extinction coefficient will also decrease. However, the exact reason for the intensity reduction of the DR and PL spectra of TNS/C10TMA/R3B hybrid by water adsorption is not clear, and further experiment and analyses will be required for discovering the exact reason.

Mechanism of Structural and Spectroscopic Response by Water Adsorption. In Figure 8, the prospective mechanism of structural and spectroscopic response by water adsorption is shown. In the dry state, C10TMA cations were aligned almost perpendicular to the TNS surface (Figure 8a), and the incorporated R3B cations were strongly fixed by electrostatic interaction between the cation-group ($-NEt_2$) of R3B and cation-exchange site on TNS surface (Figure 8b). When the

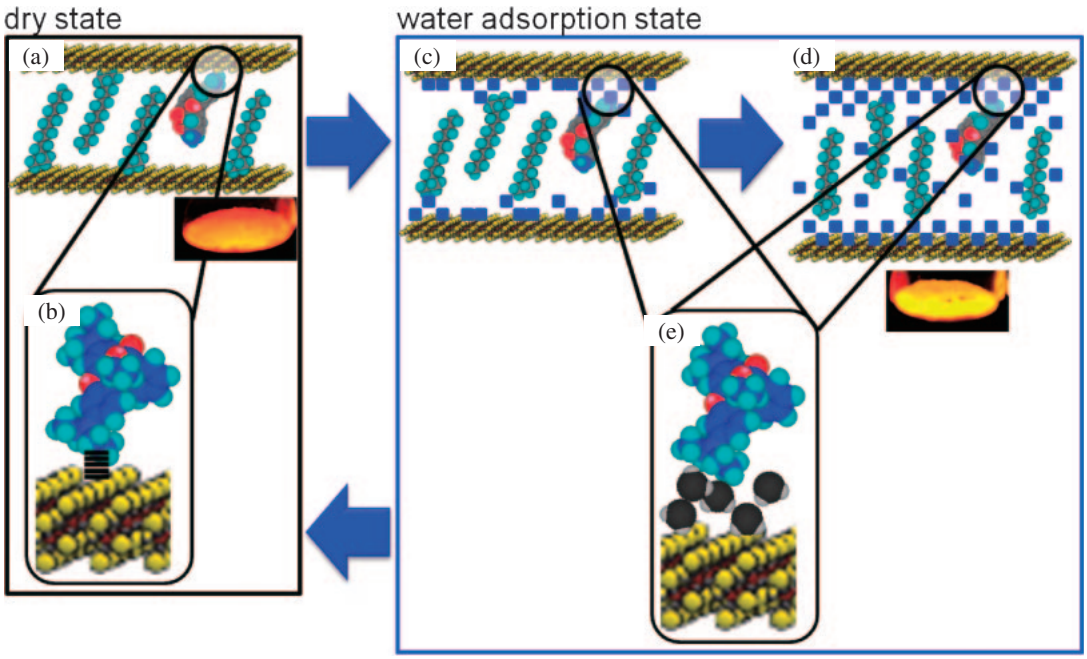

Figure 8. Prospective mechanism model of structural and spectroscopic response of TNS/C10TMA/R3B hybrids for water adsorption. Inserted photographs are luminescence appearance under black lamp (356 nm). (a) Overall structural model of TNS/C10TMA/R3B dried material. (b) Enlarged view around between R3B and TNS surface under dried condition. Overall structural model of TNS/C10TMA/R3B under (c) low RH (<20%) and (d) high RH (>20%). (e) Enlarged view around between R3B and TNS surface under humid conditions.

dried TNS/C10TMA/R3B hybrid powder is exposed to humid atmosphere, the water molecules are adsorbed onto two different water adsorption sites in the interlayer 2D nanospace of TNS stacked structure (Figures 8c and 8d). At the same time, the electrostatic interaction between the cation-group ($-NEt_2$) of R3B and cation-exchange site on TNS surface are weakened or diminished by water adsorption (Figure 8e). As a result of these phenomena, it is considerable that the PL tone-color of the TNS/C10TMA/R3B hybrid changes.

Conclusion

In this study, we could elucidate the structural and spectroscopic change of the TNS/C10TMA/R3B luminous solid hybrid powder by water adsorption as follows: (1) the TNS/C10TMA/R3B hybrid has at least two sites for water adsorption, which are a high affinity site and physisorption site with lower affinity. (2) Expansion of the interlayer clearance space of TNS stacked structure under humid atmosphere is mainly caused by water adsorption between the cation-group ($-NEt_2$) of R3B and cation-exchange site on TNS surface. At the same time, the orientation change of both C10TMA and R3B will also occur. (3) The tone-change of the TNS/C10TMA/R3B hybrid powder could be observed under humid atmosphere. This tone-change is caused by the reduction of electrostatic interaction between the cation-group ($-NEt_2$) of R3B and cation-exchange site on TNS surface by water adsorption onto high affinity water adsorption sites. As a future work, we will attempt the PL and DR spectra measurement under various RH conditions, because we are interested in more details of the luminous change properties of the present hybrid against various RH conditions.

This work was partly supported by a Grant-in-Aid for Young Scientists (B) (No. 16750172) from the Ministry of Education, Culture, Sports, Science and Technology (MEXT), by Research for Promoting Technological Seeds (FY2006, FY2007, and FY2008) of the Japan Science and Technology Agency (JST), and by Murata Science Foundation (2010).

References

1 *Kikan Kagaku Sosetsu No. 21, Microporous Crystals*, ed. by the Chemical Society of Japan, Japan Scientific Societies Press, Tokyo, **1994**.

2 M. Ogawa, K. Kuroda, *Chem. Rev.* **1995**, *95*, 399.

3 *Kikan Kagaku Sosetsu No. 42, Muki-Yuki Nano Fukugoutai Busshitsu*, ed. by the Chemical Society of Japan, Japan Scientific Societies Press, Tokyo, **1999**.

4 *Handbook of Layered Materials*, ed. by S. M. Auerbach, K. A. Carrado, P. K. Dutta, Marcel Dekker, Inc., New York, **2004**.

5 *Handbook of Clay Science*, ed. by F. Bergaya, B. K. G. Theng, G. Lagaly, Elsevier, **2008**.

6 T. Endo, T. Sato, M. Shimada, *J. Phys. Chem. Solids* **1986**, *47*, 799.

7 M. Ogawa, R. Kawai, K. Kuroda, *J. Phys. Chem.* **1996**, *100*, 16218.

8 R. Sasai, N. Shin'ya, T. Shichi, K. Takagi, K. Gekko, *Langmuir* **1999**, *15*, 413.

9 R. Sasai, T. Shichi, K. Gekko, K. Takagi, *Bull. Chem. Soc. Jpn.* **2000**, *73*, 1925.

10 R. Matsuoka, T. Yui, R. Sasai, K. Takagi, H. Inoue, *Mol. Cryst. Liq. Cryst.* **2000**, *341*, 333.

11 R. Sasai, H. Ogiso, I. Shindachi, T. Shichi, K. Takagi, *Mol. Cryst. Liq. Cryst.* **2000**, *345*, 39.

12 R. Sasai, H. Ogiso, I. Shindachi, T. Shichi, K. Takagi,

Tetrahedron **2000**, *56*, 6979.
13 H. Nishikiori, R. Sasai, N. Arai, K. Takagi, *Chem. Lett.*, **2000**, 1142.
14 R. Sasai, H. Itoh, I. Shindachi, T. Shichi, K. Takagi, *Chem. Mater.* **2001**, *13*, 2012.
15 N. Iyi, R. Sasai, T. Fujita, T. Deguchi, T. Sota, F. L. Arbeloa, K. Kitamura, *Appl. Clay Sci.* **2002**, *22*, 125.
16 R. Sasai, T. Fujita, N. Iyi, H. Itoh, K. Takagi, *Langmuir* **2002**, *18*, 6578.
17 Y. Kaneko, N. Iyi, J. Bujdák, R. Sasai, T. Fujita, *J. Colloid Interface Sci.* **2004**, *269*, 22.
18 S. Yokoyama, A. Otomo, S. Mashiko, *Appl. Phys. Lett.* **2002**, *80*, 7.
19 R. Sasai, N. Iyi, T. Fujita, K. Takagi, H. Itoh, *Chem. Lett.* **2003**, *32*, 550.
20 J. Bujdák, N. Iyi, Y. Kaneko, A. Czímerová, R. Sasai, *Phys. Chem. Chem. Phys.* **2003**, *5*, 4680.
21 R. Sasai, D. Sugiyama, S. Takahashi, Z. Tong, T. Shichi, H. Itoh, K. Takagi, *J. Photochem. Photobiol., A* **2003**, *155*, 223.
22 L. A. Lucia, T. Yui, R. Sasai, S. Takagi, K. Takagi, H. Yoshida, D. G. Whitten, H. Inoue, *J. Phys. Chem. B* **2003**, *107*, 3789.
23 R. Sasai, N. Iyi, T. Fujita, F. L. Arbeloa, V. M. Martínez, K. Takagi, H. Itoh, *Langmuir* **2004**, *20*, 4715.
24 J. Bujdák, N. Iyi, R. Sasai, *J. Phys. Chem. B* **2004**, *108*, 4470.
25 I. Shindachi, H. Hanaki, R. Sasai, T. Shichi, T. Yui, K. Takagi, *Chem. Lett.* **2004**, *33*, 1116.
26 R. Sasai, T. Itoh, N. Iyi, K. Takagi, H. Itoh, *Chem. Lett.* **2005**, *34*, 1490.
27 T. Yui, I. Shindachi, R. Sasai, K. Takagi, *Mol. Cryst. Liq. Cryst.* **2005**, *431*, 321.
28 J. Bujdák, N. Iyi, *Chem. Mater.* **2006**, *18*, 2618.
29 H. Nishikiori, R. Sasai, K. Takagi, T. Fujii, *Langmuir* **2006**, *22*, 3376.
30 I. Shindachi, H. Hanaki, R. Sasai, T. Shichi, T. Yui, K. Takagi, *Res. Chem. Intermed.* **2007**, *33*, 143.
31 J. Kawamata, R. Seike, T. Higashi, Y. Inada, J. Sasaki, Y. Ogata, S. Tani, A. Yamagishi, *Colloids Surf., A* **2006**, *284–285*, 135.
32 T. Higashi, R. Yasui, S. Tani, Y. Ogata, A. Yamagishi, J. Kawamata, *Clay Sci.* **2006**, *12*, 42.
33 J. Kawamata, S. Hasegawa, *J. Nanosci. Nanotechnol.* **2006**, *6*, 1620.
34 S. Takagi, M. Eguchi, D. A. Tryk, H. Inoue, *J. Photochem. Photobiol., C* **2006**, *7*, 104.
35 J. Bujdák, V. M. Martínez, F. L. Arbeloa, N. Iyi, *Langmuir* **2007**, *23*, 1851.
36 N. Khaorapapong, M. Ogawa, *Appl. Clay Sci.* **2007**, *35*, 31.
37 T. Okada, Y. Ehara, M. Ogawa, *Clays Clay Miner.* **2007**, *55*, 348.
38 M. Eguchi, H. Tachibana, S. Takagi, D. A. Tryk, H. Inoue, *Bull. Chem. Soc. Jpn.* **2007**, *80*, 1350.
39 S. Takagi, M. Eguchi, T. Shimada, S. Hamatani, H. Inoue, *Res. Chem. Intermed.* **2007**, *33*, 177.
40 M. Eguchi, H. Tachibana, S. Takagi, H. Inoue, *Res. Chem. Intermed.* **2007**, *33*, 191.
41 J. Kawamata, H. Yamaki, R. Ohshige, R. Seike, S. Tani, Y. Ogata, A. Yamagishi, *Colloids Surf., A* **2008**, *321*, 65.
42 R. Sasai, Y. Hotta, H. Itoh, *J. Ceram. Soc. Jpn.* **2008**, *116*, 205.
43 R. Sasai, T. Itoh, W. Ohmori, H. Itoh, M. Kusunoki, *J. Phys. Chem. C* **2009**, *113*, 415.
44 M. Fang, C. H. Kim, G. B. Saupe, H.-N. Kim, C. C. Waraksa, T. Miwa, A. Fujishima, T. E. Mallouk, *Chem. Mater.* **1999**, *11*, 1526.
45 T. Hattori, Z.-W. Tong, Y. Kasuga, Y. Sugito, T. Yui, K. Takagi, *Res. Chem. Intermed.* **2006**, *32*, 653.
46 T. Yui, Y. Kobayashi, Y. Yamada, T. Tsuchino, K. Yano, T. Kajino, Y. Fukushima, T. Torimoto, H. Inoue, K. Takagi, *Phys. Chem. Chem. Phys.* **2006**, *8*, 4585.
47 T. Nakato, Y. Yamashita, K. Kuroda, *Thin Solid Films* **2006**, *495*, 24.
48 T. Yui, T. Tsuchino, T. Itoh, M. Ogawa, Y. Fukushima, K. Takagi, *Langmuir* **2005**, *21*, 2644.
49 N. Miyamoto, K. Kuroda, M. Ogawa, *J. Phys. Chem. B* **2004**, *108*, 4268.
50 N. Miyamoto, K. Kuroda, M. Ogawa, *J. Mater. Chem.* **2004**, *14*, 165.
51 N. Miyamoto, K. Kuroda, M. Ogawa, *Mol. Cryst. Liq. Cryst.* **2000**, *341*, 259.
52 W.-W. Qu, F. Chen, B. Zhao, J.-L. Zhang, *J. Phys. Chem. Solids* **2010**, *71*, 35.
53 Â. A. Teixeira-Neto, A. L. Shiguihara, C. M. S. Izumi, M. A. Bizeto, F. Leroux, M. L. A. Temperini, V. R. L. Constantino, *Dalton Trans.* **2009**, 4136.
54 R. Shinozaki, T. Nakato, *Microporous Mesoporous Mater.* **2008**, *113*, 81.
55 K. Takada, H. Sakurai, E. Takayama-Muromachi, F. Izumi, R. A. Dilanian, T. Sasaki, *Nature* **2003**, *422*, 53.
56 K. Takada, H. Sakurai, E. Takayama-Muromachi, *Physics and Chemistry of the Cobalt Oxide Hydrate Superconductor* in *Frontiers in Superconducting Materials*, ed. by A. V. Narlikar, Splinger-Verlag, **2005**, pp. 651–682.
57 T. Sasaki, Y. Ebina, T. Tanaka, M. Harada, M. Watanabe, G. Decher, *Chem. Mater.* **2001**, *13*, 4661.
58 T. Sasaki, M. Watanabe, H. Hashizume, H. Yamada, H. Nakazawa, *J. Am. Chem. Soc.* **1996**, *118*, 8329.
59 J. C. Conboy, M. C. Messmer, G. L. Richmond, *J. Phys. Chem. B* **1997**, *101*, 6724.
60 F. L. Arbeloa, T. L. Arbeloa, I. L. Arbeloa, in *Encyclopedia of Surface and Colloid Science*, 2nd ed., ed. by P. Somasundaran, Taylor & Francis, New York, **2006**, pp. 2325–2337.
61 F. L. Arbeloa, T. L. Arbeloa, I. L. Arbeloa, in *Encyclopedia of Surface and Colloid Science*, ed. by A. Hubbard, Marcel Dekker, New York, **2002**, pp. 2007–2020.